Mössbauer spectroscopy of ^{57}Fe in α-Al$_2$O$_3$ following implantation of ^{57}Mn*

**H. P. Gunnlaugsson · R. Mantovan · T. E. Mølholt · D. Naidoo · K. Johnston ·
H. Masenda · K. Bharuth-Ram · G. Langouche · S. Ólafsson · R. Sielemann ·
G. Weyer · Y. Kobayashi · the ISOLDE collaboration**

Abstract The valence state and annealing reactions of Mn/Fe in single crystalline α-Al$_2$O$_3$ have been determined following low fluence ($<10^{12}$ cm^{-2}) 60 keV implantations of ^{57}Mn$^+$ ($T_{1/2} = 1.5$ min) and emission Mössbauer spectroscopy on the ^{57m}Fe daughter nuclei in the temperature range from 110–700 K. At 110 K, most probe atoms are found in the Fe^{2+} state in amorphous surroundings due to the implantation damage. A fraction of the Fe is found in cubic environment, possibly nano-precipitates of η-Al$_2$O$_3$. This site is found to disappear from the

H. P. Gunnlaugsson (✉) · G. Weyer
Department of Physics and Astronomy, Aarhus University, 8000 Århus C, Denmark
e-mail: hpg@phys.au.dk

R. Mantovan
Laboratorio MDM, IMM-CNR, Via Olivetti 2, 20041 Agrate Brianza (MB), Italy

T. E. Mølholt · S. Ólafsson
Science Institute, University of Iceland, Dunhaga 3, 107 Reykjavík, Iceland

D. Naidoo · H. Masenda
School of Physics, University of the Witwatersrand, Private Bag 3, WITS 2050, South Africa

K. Johnston · the ISOLDE collaboration
PH Dept, ISOLDE/CERN, 1211 Geneva 23, Switzerland

K. Bharuth-Ram
School of Physics, University of KwaZulu-Natal, Durban 4001, South Africa

G. Langouche
Instituut voor Kern- en Stralingsfysica, University of Leuven, 3001 Leuven, Belgium

R. Sielemann
Helmholtz-Zentrum Berlin für Materialien und Energie, 14109 Berlin, Germany

Y. Kobayashi
The Institute of Physical and Chemical Research (RIKEN), Wako, Saitama 351-0198, Japan

spectra above 500 K. Annealing of the damage sites at increasing temperatures leads first to increased incorporation of the probe atoms as Fe^{3+} on Al sites, and, above room temperature, also as Fe^{4+}. The Fe^{3+} sub-spectrum is masked by slow paramagnetic relaxations following a T^2 dependence, as expected for a two-phonon Raman process. Our data is consistent with data from ^{57}Co and ^{57}Fe implantations, suggesting a general increase in the average Fe valence state with lower implantation dose and negligible annealing reactions at room temperature.

1 Introduction

Mössbauer spectroscopy of Fe impurities in α-Al_2O_3 has been of interest for the last four decades with some of the pioneering Mössbauer work on slow paramagnetic relaxations of Fe^{3+} impurities being performed in this material [1–3]. Several authors [4–6] claimed that upon high fluence implantation ($\sim 10^{17}$ $^{57}Fe/cm^2$) Fe was observed in the 4+ valence state. This claim was disproved by low temperature measurements of Kobayashi et al. [7] where it was shown that the spectral features assigned to Fe^{4+} were due to fine particles of metallic iron.

The fluence dependence of the ^{57}Fe Mössbauer spectrum upon implantation has been described by several authors. McHargue et al. [8] reported the fluence dependence in the range 10^{16}–10^{17} $^{57}Fe/cm^2$, after implantation of 100–160 keV ^{57}Fe at room temperature. They observed a gradual change from an Fe^{2+} dominated spectrum to a spectrum dominated by uncharged iron. Dézsi et al. [9] performed 80 keV ^{57}Co implantations to fluences of $(1–3) \times 10^{14}$ $^{57}Co/cm^2$ and observed Fe in the 3+ and 2+ charge states, together with a single line of unknown origin.

Here we present results obtained after 60 keV implantation of $^{57}Mn^+$ ($T_{1/2} = 1.5$ min) performed at ISOLDE/CERN and emission ^{57}Fe Mössbauer spectroscopy on the daughter nuclei. The outstanding feature of this method, in the context of previous work, is the low total fluence needed to obtain a useful spectrum. The total fluence the sample received is of the order of $\sim 10^{12}$ $^{57}Mn/cm^2$.

2 Experimental

Beam of radioactive $^{57}Mn^+$ ($T_{1/2} = 1.5$ min) ions is produced at the ISOLDE facility at CERN following proton induced fission in UC_2 target and element selective laser ionization [10]. The ions have been implanted into single crystals of α-Al_2O_3 with an intensity of $(1–3) \times 10^8$ s^{-1} of $^{57}Mn^+$ to a total fluence of $\leq 10^{12}$ $^{57}Mn/cm^2$. In the β^- decay of ^{57}Mn, the daughter nuclei are given a recoil of average energy $\langle E_R \rangle = 40$ eV. The samples were mounted in an implantation chamber with the c-axes tilted 30° relative to the beam direction and the detector mounted at 60° relative to the c-axis of the orthorhombic Al_2O_3 lattice. For measurements above room temperature, the samples were heated with a Halogen lamp from behind. For measurements below RT the samples were mounted on a cold finger cooled with N_2 gas.

^{57}Fe Mössbauer spectra were measured with resonance detectors equipped with stainless steel electrodes enriched in ^{57}Fe. The detector is mounted on a conventional
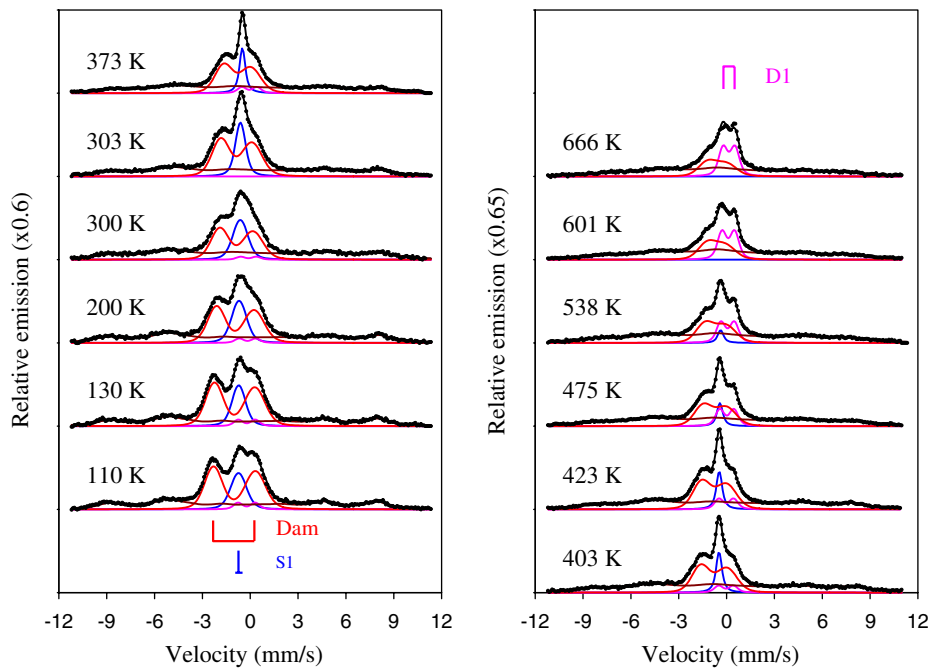
Fig. 1 ^{57}Fe Mössbauer spectra obtained after implantation of ^{57}Mn$^+$ at the temperatures indicated. The *lines* indicate the fitting components explained in the text

drive system outside the implantation chamber. The intrinsic line-shape of the detector is best analyzed in terms of Voigt profiles with a Lorentzian width of 0.34 mm/s and Gaussian broadening of 0.08 mm/s. Isomer-shifts and velocities are given at room temperature relative to α-Fe.

3 Results and analysis

The spectra obtained at different temperatures are shown in Fig. 1. Measurements after implantation fluencies ranging from 10^{10} to 10^{11} ^{57}Mn/cm^2 at room temperature did not reveal any fluence dependence of the spectral components as has been reported in similar experiments in ZnO [11] and attributed to the mobility of intrinsic defects at room temperature.

In these on-line measurements, the total implantation increases with successive measurements. The spectrum observed at 403 K was measured after the series of high temperature measurements in the range 303–666 K. Its spectral features follow the systematic trend of the other temperature dependent spectra and verify the lack of any dependence on implantation fluence.

Below and at room temperature, the central part of the spectra is dominated by an asymmetric quadrupole doublet (Dam). The rather broad lines of this component suggest it is due to Fe in damage sites due to the implantation. Similar asymmetrically broadened quadrupole doublets due to implantation damage have been observed after implantation of ^{57}Mn into group IV semiconductors [12–15]. Additionally,
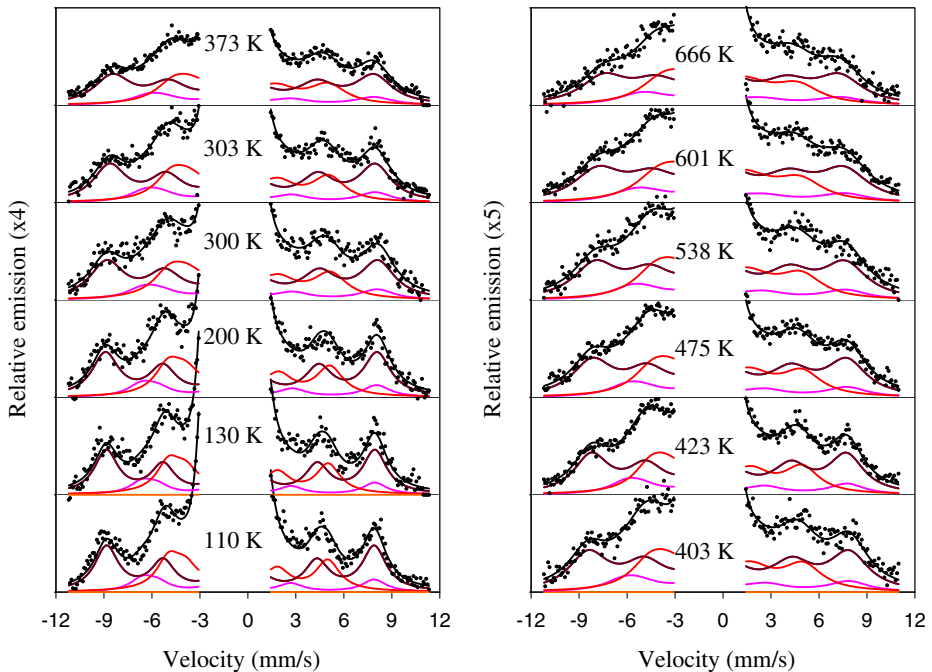
Fig. 2 The same spectra as in Fig. 1, but with the central part removed and the vertical scale expanded to reveal the structure in the outer flanks

the central part of the spectra contains a single line (S1) with room temperature parameters similar to those observed by Dézsi et al. [9]. Below room temperature, this line shows broadening and disappears from the spectra at $T > 500$ K. At $T > 600$ K, the central part of the spectra is dominated by a quadrupole doublet (D1). Due to the fact that this component only dominates the spectra in a relatively small temperature interval, its quadrupole splitting was restricted to follow a $T^{3/2}$ temperature dependence in the analysis. Spectra obtained at different emission angles at room temperature did not reveal any angular dependence of the doublet components.

In Fig. 2, we focus on the outer flanks of the spectra. The wings of the spectra show an asymmetric pattern (higher intensity on the left hand side), similar to that noted in ZnO [16, 17] and MgO [18]. The high maximum magnetic hyperfine field splitting ($\sim$50 T) unambiguously determines the origin of this component being due to Fe^{3+}.

The spectral changes at elevated temperatures of the wings of the spectra are most likely due to increasing relaxation rates and were analyzed with the semi-empirical relaxation model described by Mølholt et al. [18]. In the case of Al_2O_3, it is assumed that the temperature dependent relaxation rate is negligible at 110 K and three relaxation sextets proved adequate to explain the spectral shape.

The final analysis was performed simultaneously where the line-widths were set to temperature independent constants and line positions set to follow the second order Doppler shift (except for S1 at $T < 300$ K). The Mössbauer fit parameters,

Table 1 Hyperfine parameters obtained from the simultaneous analysis of the spectra in Fig. 1

	δ (mm/s)	ΔE_Q (mm/s)	σ (mm/s)	
S1	0.546 (4)	0	0.087 (5)[c]	
D1	0.107 (5)	0.99 (3)[b]	0.195 (4)	
Dam[a]	0.869 (6)	2.0 (1)	0.484 (4)	0.563 (9)
Para. Fe^{3+}	0.35 (1)	n/a	n/s	

The table lists isomer shift (δ) and quadrupole splitting (ΔE_Q) at room temperature and Gaussian broadening (σ). All lines were analyzed using the Voigt profile with a Lorentzian broadening of 0.34 mm/s

[a] σ given for left and right legs, respectively

[b] At room temperature

[c] Observed broader ($\Delta\sigma \sim 0.30(5)$ mm/s) below room temperature, the value given here obtained at $T \geq 300$ K

Fig. 3 Spin-relaxation rate obtained by fit to the semi-empirical relaxation model described in [18] compared to a T^2 law
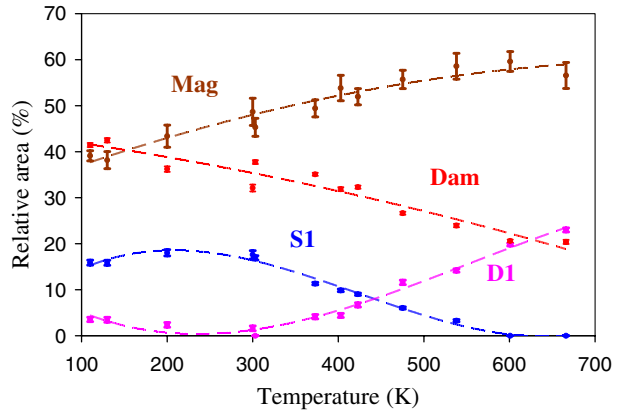

isomer shift (δ), quadrupole splitting (ΔE_Q) at room temperature and Gaussian broadening (σ), are listed in Table 1. All lines were analyzed using a Voigt profile with a Lorentzian broadening of 0.34 mm/s. The quadrupole splitting of D1 was set to follow $\Delta E_Q = \Delta E_{Q,0}(1 - (T/T_k)^{3/2})$ and the values $\Delta E_{Q,0} = 1.09(4)$ mm/s and $T_k = 1,400(100)$ K were determined. The maximum hyperfine splitting of the paramagnetic Fe^{3+} component was found to decrease by 10(2) % between 110 K and 600 K.

The relaxation rates obtained for the paramagnetic Fe^{3+} at the different temperatures are shown in Fig. 3. The temperature dependence can easily be compared with a T^2 dependence suggesting a Raman process for the spin lattice relaxation as expected at $T > \theta_D/4$, where θ_D is the Debye temperature.

The area fractions obtained from the analysis are shown in Fig. 4. The total spectral area reduces in almost a linear way from 110 K to 666 K by a factor of 0.66, suggesting an average Debye temperature of ~450 K. There are no features in the total area that can be related to strong differences in the Debye temperatures of the appearing/disappearing fractions (S1 and D1).

Fig. 4 Area fractions of the spectral components determined from the simultaneous analysis. *Dashed lines* are to guide the eye
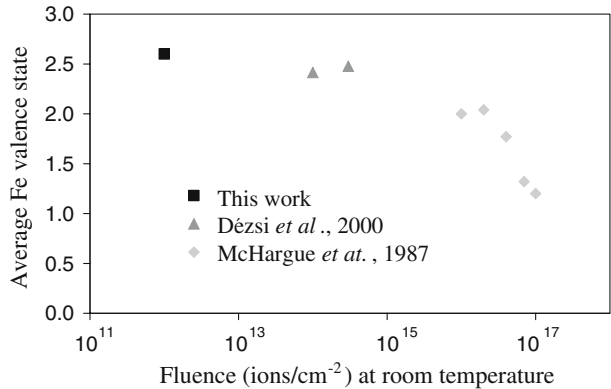

4 Discussion

At low temperatures the spectra are dominated by a broad-lined component (Dam). Its isomer shift indicates that it is due to Fe^{2+}. The broad line width and asymmetry of this component is due to a correlated distribution of isomer shifts and quadrupole splittings at the Fe sites and is most probably a consequence of the probe atoms being incorporated in amorphous pockets, similar to observations in silicon [13]. Damaged sites with similar properties have been observed in other types of materials upon implantation of ^{57}Mn [12–15]. The area fraction of the damage decreases from ~42% at 110 K to 20% at ~650 K showing that the probability of ending up in such a site is lower at elevated temperatures or it anneals within the Mn lifetime.

The straight-forward interpretation of the single line (S1) would be to assign it to interstitial Fe owing to the average 40 eV recoil imparted on the Fe daughter nuclei in the β^- decay of ^{57}Mn. However, there are several inconsistencies in such an interpretation. The disappearance of this component above 500 K, would suggest that the interstitial site is not stable over the lifetime of the Mössbauer state ($\tau = 140$ ns), and the interstitial atom is incorporated onto a regular lattice site at times shorter than 100 ns above 500 K. Such transformation should lead to broadening of the interstitial line due to the effective shortening of the lifetime of the atom in the interstitial site relative to the lifetime of the Mössbauer state [19]. This, however, is not supported by the experimental data at $T \leq 475$ K.

A similar (if not identical) single line component ($\delta = 0.54$–0.55 mm/s) was observed in the ^{57}Co data of Dézsi et al. [9]. In the electron capture of ^{57}Co, only a minor (<1 eV) recoil is imparted on the ^{57}Fe daughter nuclei, so it seems unlikely that S1 originates from a recoil produced ^{57}Fe. These authors suggested that this component originates from a mixed valence state. ^{57}Co decays dominantly by electron capture, which leaves the daughter atom in a highly excited electronic state, often giving rise to after-effects and unusual charge states (see e.g. discussion in Ref. [20]). The β^- decay of ^{57}Mn on the other hand does not alter the electronic structure significantly and the creation of unusual charge states is unlikely.

The S1 component shows broadening and a possible small change in isomer-shift below room temperature. Such behaviour could be explained as due to lattice imperfections at low temperatures, where no, or only limited, annealing of damage

Fig. 5 Average valence
state of Fe as a function
of implantation fluence
in α-Al$_2$O$_3$

due to the implantation takes place around the probe atom. Due to less binding of
interstitial Fe to the lattice, less pronounced low temperature broadening would be
expected.

The S1 component shows no significant broadening above 500 K and has negli-
gible quadrupole interaction ($|\Delta E_Q| < 0.02$ mm/s, determined from lack of angular
dependence). Interstitial sites in α-Al$_2$O$_3$ would be expected to give rise to detectable
quadrupole splitting due to the rhombohedral lattice.

An alternative possibility for the origin of this line is that the Mn atom leads to
a formation of another crystal structure upon re-crystallisation of the amorphous
pockets. One possibility is the cubic η-Al$_2$O$_3$, but the data presented here is not
able to distinguish one structure from another. XRD measurements on implanted
material could test for the presence of precipitates of η-Al$_2$O$_3$ if it can be formed
under low fluence ($<10^{15}$ cm^{-2}) implantations.

At temperatures above room temperature, a new component D1 is observed, with
an isomer-shift consistent with both Fe^{3+} and Fe^{4+}. It would, however, seem to be a
contradiction to have both a fast relaxation Fe^{3+} species (relaxation rates $> 10^{11}$ s^{-1})
and a slow relaxation Fe^{3+} (relaxation rates $< 10^8$ s^{-1}, cf. Fig. 3) species in the
same temperature range. Furthermore, the parameters of D1 are not consistent with
parameters of fast relaxing paramagnetic Fe^{3+} either in α-(Al,Fe)$_2$O$_3$ solid solutions
[21] or from implanted material [8]. Hence the interpretation of D1 as due to Fe^{4+} is
favoured. It should be noted that this component has no relationship to the proposed
Fe^{4+} components claimed by other authors [4–6] upon high fluence implantation.

One could suspect that this component was due to interstitial Fe. However,
recoil produced interstitial Fe is more likely to have decreasing spectral area due
to lower average Debye temperatures, or disappear due to instability at elevated
temperatures. If D1 were due to interstitial Fe, one would expect drastic changes in
the total area at elevated temperatures, which is not observed. We therefore favour
the origin of this component as due to Fe^{4+}, even though interstitial Fe formed upon
annealing of the cubic site (S1) can not be excluded.

Together with the data from [8] and [9], we can extend the range in implantation
fluence, where the average valence state of Fe is determined. The results are shown
in Fig. 5.

Generally, lower fluence implantations result in higher average valence state of
Fe. At higher temperatures, the average valence state of Fe increases up to $\sim$3

(assuming D1 originates from Fe^{4+}), mostly due to annealing of Fe^{2+} damaged sites and incorporation of the probe atoms onto sites with higher valence state. For fluences above $\sim 10^{14}$ cm^{-2}, the material becomes completely amorphous, and this state is apparently characterized with Fe^{2+}. For fluences above $\sim 10^{16}$ cm^{-2} spontaneous formation of metallic precipitates takes place, and average valence state below 2+ are observed.

These findings are generally similar to those of Perez et al. [22] upon implantation into MgO. They found Fe^{3+} as the dominating species following 3×10^{15} ^{57}Fe/cm^2 implanted at 100 keV. Fe^{2+} became the dominating species at $\sim 2 \times 10^{16}$ ^{57}Fe/cm^2, and metallic iron started to dominate the spectra at $\sim 7 \times 10^{16}$ ^{57}Fe/cm^2.

The general tendency seen in this data, spanning roughly five decades in implantation fluence suggests no or very limited annealing reactions in α-Al$_2$O$_3$. In our ^{57}Mn experiments, the Mössbauer data is obtained few minutes after implantation, while in ^{57}Co and ^{57}Fe experiments, the data is obtained $\sim$days/weeks after the implantation, and there is no evidence of major changes in lattice fractions on this timescale.

5 Conclusions

The Mössbauer spectrum of ^{57}Fe following implantation of ^{57}Mn into single crystalline α-Al$_2$O$_3$ has been measured in low fluence implantations ($\leq 10^{12}$ ^{57}Mn/cm^2) in the temperature range from 110–700 K.

At 110 K roughly 40% of the spectral area is assigned to probe atoms found in the Fe^{2+} state in amorphous surroundings owing to the implantation damage. A fraction of the Fe is found in cubic environment, possibly due to nano-precipitates of η-Al$_2$O$_3$which disappear from the spectra above 500 K.

Incomplete annealing of the damaged sites at increasing temperatures leads first to incorporation of the probe atoms in Fe^{3+} valence state, and above room temperature most likely as Fe^{4+}. The Fe^{3+} sub-spectrum is masked by slow paramagnetic relaxations, following T^2 dependence, characteristic for a two-phonon Raman process.

Our data is consistent with data from ^{57}Co and ^{57}Fe implantations, suggesting a general increase in valence state with lower implantation fluence.

References

1. Wertheim, G.K., Remeika, J.P.: Mössbauer effect hyperfine structure of trivalent Fe^{57} in corundum. Phys. Lett. **10**, 14–15 (1964)
2. Wickman, H.H., Wertheim, G.K.: Mössbauer hyperfine spectra of Fe^{3+} in corundum: magnetic- and crystal-field effects. Phys. Rev. B **148**, 211–217 (1966)
3. Hess, J., Levy, A.: Response of the Mössbauer spectrum of paramagnetic Fe^{3+} in Al$_2$O$_3$ to nuclear dipole fields. Phys. Rev. B **22**, 5068–5078 (1980)
4. Donnet, C., Jaffrezic, H., Marest, G., Moncoffre, N., Tousset, J.: Iron-implantation sintered alumina studied by RBS, CEMS and SEM techniques. Nucl. Instrum. Methods B **50**, 410–415 (1990)

5. McHargue, C.J., Sklad, P.S., McCallum, J.C., White, C.W., Ferez, A., Marest, G.: The structure of Al$_2$O$_3$ implanted with iron at 77 K. Nucl. Instrum. Methods B **46**, 144–148 (1990)

6. Guomei, W., Shipu, L., Ning, X., Donghui, F.: Structure and surface properties of polycrystalline ^{57}Fe implanted aluminas. Nucl. Instrum. Methods B **72**, 64–68 (1992)

7. Kobayashi, T., Nakanishi, A., Fukumura, K., Langouche, G.: Fine iron particles formed in a sapphire crystal by the ion implantation technique. J. Appl. Phys. **83**, 4631–4641 (1998)

8. McHargue, C.J., Farlow, G.C., Sklad, P.S., White, C.W., Perez, A., Kornilios, N., Marest, G.: Iron ion implantation effects in sapphire. Nucl. Instrum. Methods B **19/20**, 813–821 (1987)

9. Dézsi, I., Szűcs, I., Fetzer, Cs., Pattyn, H., Langouche, G., Pfannes, H.D., Magalhães-Paniago, R.: Local interactions of ^{57}Fe after electron capture of ^{57}Co implanted in α-Al$_2$O$_3$ and in α-Fe$_2$O$_3$. J. Phys., Condens. Matter **12**, 2291–2296 (2000)

10. Fedoseyev, V.N., Bätzner, K., Catherall, R., Evensen, A.H.M., Forkel-Wirth, D., Jonsson, O.C., Kugler, E., Lettry, J., Mishin, V.I., Ravn, H.L., Weyer, G., the ISOLDE Collaboration: Chemically selective laser ion source of manganese. Nucl. Instrum. Methods B **126**, 88–91 (1997)

11. Mølholt, T.E., Mantovan, R., Gunnlaugsson, H.P., Bharuth-Ram, K., Fanciulli, M., Gíslason, H.P., Johnston, K., Kobayashi, Y., Langouche, G., Masenda, H., Naidoo, D., Ólafsson, S., Sielemann, R., Weyer, G.: Temperature and dose dependence of defect complex formation with ion-implanted Mn/Fe in ZnO. Physica B **404**, 4820–4822 (2009)

12. Gunnlaugsson, H.P., Fanciulli, M., Dietrich, M., Baruth-Ram, K., Sielemann, R., Weyer, G., the ISOLDE collaboration: ^{57}Fe Mössbauer study of radiation damage in ion implanted Si, SiGe and SiSn. Nucl. Instum. Methods B. **168**, 55–60 (2002)

13. Weyer, G., Gunnlaugsson, H.P., Dietrich, M., Fanciulli, M., Baruth-Ram, K., Sielemann, R., the ISOLDE collaboration: Creation and annealing of defect structures in silicon-based semiconductors during and after implantation at 77–500 K. Nucl. Instrum. Methods B **206**, 90–94 (2003)

14. Weyer, G., Gunnlaugsson, H.P., Dietrich, M., Fynbo, H., Bharuth-Ram, K., the ISOLDE Collaboration: Mössbauer spectroscopy on Fe impurities in diamond. Eur. Phys. J. Appl. Phys. **27**, 317–320 (2004)

15. Gunnlaugsson, H.P., Bharuth-Ram, K., Dietrich, M., Fanciulli, M., Fynbo, H.O.U., Weyer, G.: Identification of substitutional and interstitial Fe in 6H-SiC. Hyp. Int. **169**, 1318–1323 (2006)

16. Weyer, G., Gunnlaugsson, H.P., Mantovan, R., Naidoo, D., Bharuth-Ram, K., Fanciulli, M., Agne, T.: Defect-related local magnetism at dilute Fe atoms in ion-implanted ZnO. J. Appl. Phys. **102**, 113915 (2007)

17. Gunnlaugsson, H.P., Mølholt, T.E., Mantovan, R., Masenda, H., Naidoo, D., Dlamini, W.B., Sielemann, R., Bharuth-Ram, K., Weyer, G., Johnston, K., Langouche, G., Ólafsson, S., Gíslason, H.P., Kobayashi, Y., Yoshida, Y., Fanciulli, M., the ISOLDE Collaboration: Paramagnetism in Mn/Fe implanted ZnO. Appl. Phys. Lett. **97**, 142501 (2010)

18. Mølholt, T.E., Mantovan, R., Gunnlaugsson, H.P., Bharuth-Ram, K., Fanciulli, M., Johnston, K., Kobayashi, Y., Langouche, G., Masenda, H., Naidoo, D., Ólafsson, S., Sielemann, R., Weyer, G., Gíslason, H.P.: Mössbauer study of spin-lattice relaxations of dilute Fe^{3+} in MgO. Hyp. Int. (2010, this conference)

19. Kankeleit, E.: The effect of decaying atomic states on integral and time differential Mössbauer spectra. Zeit. Physik. A. **275**, 119–121 (1975)

20. Gerard, A., Lerho, M.: Fe^{1+} and charge transfer in ZnS. Analysis of source experiments results. Hyp. Int. **29**, 1373–1376 (1986)

21. de Resende, V.G., Cordier, A., De Grave, E., Laurent, C., Eeckhout, S.G., Giuli, G., Peigney, A.M., da Costa, G., Vandenberghe, R.E.: Presence of metallic Fe nanoclusters in α-(Al,Fe)$_2$O$_3$ solid solutions. J. Phys. Chem. C. **112**, 16256–16263 (2008)

22. Perez, A., Marest, G., Sawicka, B.D., Sawicki, J.A., Tyliszczak, T.: Iron-ion-implantation effects in MgO crystals. Phys. Rev. B. **28**, 1227–1238 (1983)